

# Tensile and Fatigue Properties of Single and Multiple Dissimilar Welded Joints of DP980 and HSLA

Q.L. Cui, D. Parkes, D. Westerbaan, S.S. Nayak, Y. Zhou, D.C. Saha, D. Liu, F. Goodwin, S. Bhole, and D.L. Chen

(Submitted July 6, 2016; in revised form November 1, 2016; published online January 5, 2017)

The present study focused on single and multiple dissimilar joints between DP980 and high-strength low-alloy (HSLA) galvanized steels. The tensile properties of the dissimilar joint between the strong DP980 and the relatively soft HSLA reflected only the properties of HSLA with plastic deformation, and final fracture took place entirely in HSLA. The fatigue properties of the dissimilar joints were more intriguing, with the strong DP980 outperforming at high stress amplitude and the ductile HSLA outperforming at low stress amplitude. For different load amplitudes, fatigue failure occurred in different materials and at different locations. The fatigue strength of DP980 was more negatively impaired by weld defects than that of HSLA.

**Keywords** AHSS, dissimilar joint, DP steel, fatigue, fiber laser welding, HSLA, tensile strength

## 1. Introduction

With the increase in fuel consumption and greenhouse gas emission, environmental safety is becoming a social problem. The automotive industry is under constant pressure to improve fuel efficiency by reducing the weight of vehicles (Ref 1, 2). One of the solutions involves a tailor-welded blank (TWB), which involves various material options being welded together prior to the forming process. Such a concept of combining the available material options into a welded blank enables engineers to “tailor” the final part so that the best properties of materials are located precisely within the part where they are needed (Ref 3, 4). Dual-phase (DP) steel is one of the most popular types of advanced high-strength steels (AHSS) in the automotive industry owing to its high tensile strength in conjunction with high elongation compared to the steel grades of similar yield strength (Ref 5-7). On the other hand, high-strength low-alloy (HSLA) steel is a commonly used automotive steel, which consists of fine ferrite grains with dispersed ultra-fine alloy carbides (Ref 8, 9). In many applications, these two materials were welded together. Fiber laser welding (FLW) produced the best quality welds at the lowest cost to the manufacturer due to its smaller beam divergence, low main-

tenance costs, higher efficiency, high precision and reliability, and compact size (Ref 10-14).

An increased understanding of how a dissimilar welded joint behaves would be highly beneficial. A lot of research has gone into the phenomena that occur when welding DP and HSLA steels using various welding techniques (Ref 7-9, 14-17). To facilitate the design of laser-welded blanks and promote a widespread use of DP steels in the automotive industry, the relationships between the microstructural change involved in FLW and the performance of the welded joints must be evaluated so as to guarantee the reliability and durability of the parts as well as the overall safety of the passenger vehicles. In this regard, the authors (Ref 8, 16) have recently reported a study on the mechanical behavior of FLW DP980 and HSLA steels in single dissimilar combinations and multiple similar welding of DP980, and most recently, the effect of two types of zinc coatings on the fatigue properties of DP980 similar joints was published (Ref 18). It is the objective of this study to assess the tensile and fatigue properties of dissimilar multiple laser welds.

## 2. Material and Experimental Procedure

Galvanized sheet steels of DP980 and HSLA, both with a thickness of 1.2 mm, were used in this study. Their chemical compositions are listed in Table 1. Butt welding of galvanized sheets was carried out at the University of Waterloo using an IPG Photonics YLS-6000 fiber laser system attached to a Panasonic robotic arm. The welding speed was 20.5 m/min, and the laser power was 4 kW and was welded autogenously.

Metallographic samples were cut from the weld cross section, then mounted, ground, polished, and etched with a 2% Nital solution. The etched samples were observed using a light microscope and a scanning electron microscope (SEM, JEOL JSM-6380). Vickers microhardness was measured on the polished samples across the weld using a computerized microhardness tester with a load of 200 g and a dwell time of 15 s. Care was taken to prevent any potential effect of localized strain hardening caused by adjacent indentations. To ensure the accuracy of each test result, two calibration tests were performed using a standard reference test block before the microhardness tests on the welded joints were conducted.

Q.L. Cui, State Key Laboratory of Rolling and Automation, Northeastern University, 3-11 Wenhua Road, Shenyang, China and Department of Mechanical and Industrial Engineering, Ryerson University, 350 Victoria Street, Toronto, Ontario M5B 2K3, Canada; D. Parkes, S. Bhole, and D.L. Chen, Department of Mechanical and Industrial Engineering, Ryerson University, 350 Victoria Street, Toronto, Ontario M5B 2K3, Canada; D. Westerbaan, S.S. Nayak, Y. Zhou, and D.C. Saha, Department of Mechanical and Mechatronics Engineering, University of Waterloo, 200 University Avenue West, Waterloo, Ontario N2L 3G1, Canada; D. Liu, Teck Metals Ltd, 2380 Speakman Drive, Mississauga, ON L5K 1B4, Canada; F. Goodwin, International Zinc Association, Durham, NC 27713. Contact e-mails: qinglingcui@hotmail.com and Daniel.Liu@teck.com.

Tensile and fatigue test specimens of DP980-HSLA dissimilar joints were machined from a blank welded together by two 100 mm × 200 mm sheets, as shown in Fig. 1(a). The geometry and dimensions of the specimens were in compliance with ASTM: E8/E8M standard. Specimens of DP980-HSLA-DP980 multiple joint were machined from a blank with three sheets welded together, as shown in Fig. 1(b). Tensile tests were conducted on a fully computerized uniaxial tensile testing machine at room temperature and with a strain rate of  $1 \times 10^{-3} \text{ s}^{-1}$ . An extensometer with a gauge length of 50 mm and a strain limit of 20% was used to measure the strain during the tensile tests. Load control fatigue tests were performed following ASTM: E466 on a fully computerized Instron 8801 servo-hydraulic testing system. Tension-tension cyclic loading was used to prevent potential buckling of the specimens; a stress ratio of 0.1 was selected. A load with a sinusoidal waveform and a frequency of 50 Hz were employed. A minimum of two duplicates were tested in the tensile test and in the fatigue test at each of the cyclic stress amplitude. The fatigue fracture surfaces were carefully examined using SEM to explore the fatigue fracture mechanism.

### 3. Results and Discussion

#### 3.1 Microhardness

Vickers hardness (HV) measurements across a weldment reflect the underlying microstructure in the fusion zone (FZ), heat-affected zone (HAZ), and base metal (BM). Furthermore, hardness is, in general, inversely associated with impact toughness, which significantly influences the propagation of fatigue cracks (Ref 19, 20).

A typical hardness profile across a dissimilar joint between DP980 and HSLA is shown in Fig. 2. For comparison, hardness profiles of similar joints of DP980 and of HSLA are also presented. Two light-blue vertical dashed lines in the center of the graph indicated the typical width of a FZ, which was 0.57 mm as measured digitally from several SEM micrographs, as shown in Fig. 3. The measurement agreed well with the nominal laser spot size of 0.6 mm. The hardness of all three different joints was at or near their peak values in the FZ where full martensitic microstructure was obtained (Fig. 3e). The hardness of DP980 FZ was, however, higher than

**Table 1 Chemical composition of the DP980 and HSLA steels**

Steel	C	Mn	Si	Al	Cr	Ni	Mo	Nb	N	Cu	Ti
DP980	0.15	1.45	0.33	0.05	0.02	0.01	0.002	0.001	0.01	0.02	0.002
HSLA	0.08	0.8	0.46	0.05	0.03	0.01	0.003	0.04	0.01	0.04	0.002

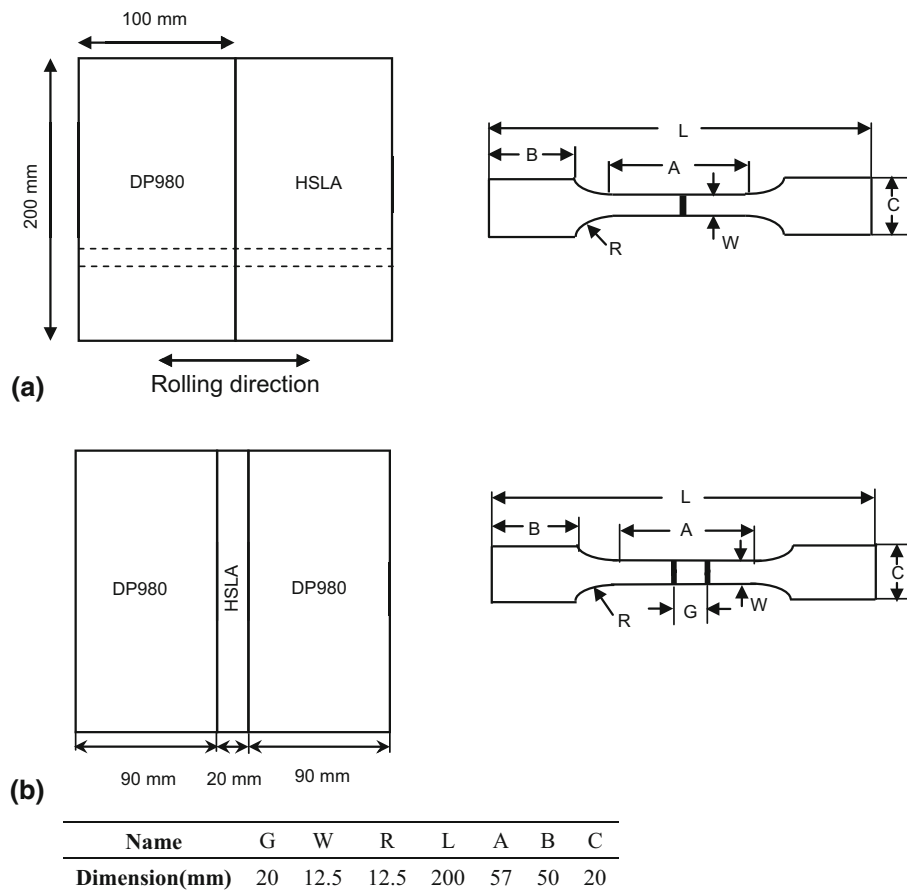


**Fig. 1** (a) Geometry of the single-line welded sheet, with transverse tensile joint machined from the dotted line, (b) geometry of the multiple-line welded sheet

that of HSLA FZ, primarily because of the higher C content of the former. Note that high hardness is often related to low impact toughness, which may aid the propagation of fatigue cracks particularly under low cyclic loads.

The hardness of DP980 in the upper-critical HAZ (ucHAZ) was also high because a fully martensitic microstructure was obtained (Fig. 3d). Owing to a low Ac<sub>3</sub> temperature (822.9 °C for DP980 versus 873.8 °C for HSLA) and good hardenability, a relatively wide plateau of high hardness with a width of about 0.2 mm was obtained for DP980 as marked by an orange dotted line in Fig. 2 for that particular weld. The borderline between ucHAZ and the inter-critical HAZ (icHAZ) was distinctly defined by the respective absence and presence of ferrite grains and was easily distinguished by metallographic examination.

Outside of the ucHAZ was icHAZ where the peak temperature lays between Ac<sub>1</sub> and Ac<sub>3</sub> temperatures (Fig. 3c). A partial martensitic microstructure was thereby obtained (Ref 15). This microstructure was similar to the dual-phase microstructure in DP980 BM where a mixture of ferrite and martensite was achieved by inter-critical annealing. However, the martensite/ferrite ratio in icHAZ decreased with decreasing peak temperature as predicted by the phase diagram. Reflecting the change from an almost fully martensitic microstructure near Ac<sub>3</sub> to a microstructure containing a significant amount of ferrite near Ac<sub>1</sub>, the microhardness in the icHAZ decreased sharply from near the peak value to a low value near the valley as shown in Fig. 2 and marked by the green vertical line for the DP980 similar weld. As for HSLA, this partial martensitic microstructure was significantly harder than the all-ferrite microstructure in its BM.

On the outskirts of HAZ was the sub-critical HAZ (scHAZ) where the peak temperature was lower than Ac<sub>1</sub> yet high enough to cause the tempering of martensite (Fig. 3b). The tempering lowered the hardness and strength of martensite while improving its toughness. The softened zone of DP980 had a width of about 0.6 mm and is prominently shown in Fig. 2 and is marked by the darker blue vertical line. On the contrary, no apparent softening occurred to HSLA due to the lack of a martensitic microstructure. Note that the tempering effect in scHAZ was increasingly severe with a decreasing distance from icHAZ; a monotonic decrease in hardness was therefore expected. The increase in the measured hardness inside scHAZ near icHAZ (Fig. 2) was likely a result of

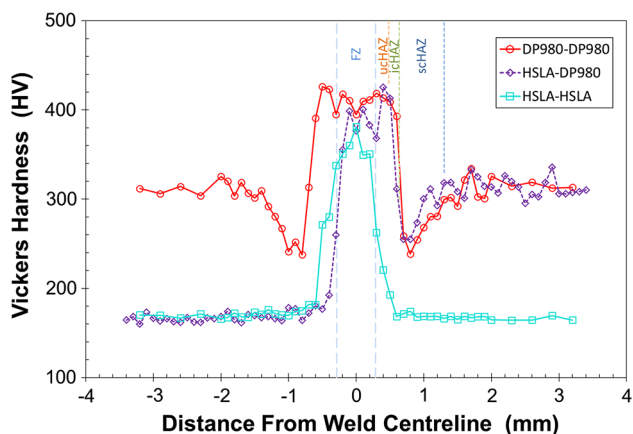


**Fig. 2** Vickers hardness measurements of similar and dissimilar welded joints

interference by the neighboring harder icHAZ, considering that the size of indentation was 40 μm at 240HV.

The hardness profile of the dissimilar HSLA-DP980 joint was, as expected, comparable to that of HSLA on the left-hand side of the joint while similar to that of DP980 on the right-hand side. In the FZ, the hardness value was higher than that of HSLA but lower than that of DP980, suggesting that the chemistry in the FZ was mixed. The highest hardness value was, unsurprisingly, recorded in ucHAZ of DP980 because its chemical composition was fully preserved.

### 3.2 Tensile Properties

Like Vickers hardness test, the tensile test provides additional information about the welds of DP980 and HSLA. Plots of engineering stress versus engineering strain for DP980 BM, HSLA BM, DP980-DP980 similar joint, DP980-HSLA dissimilar joint and DP980-HSLA-DP980 multiple joint are displayed in Fig. 4. The plot for HSLA-HSLA similar joint is not presented because of its similarity to the plot for HSLA BM. The tensile properties of HSLA-HSLA similar joint are, however, listed in Table 2 together with the results of all other specimens. Although only one representative curve is shown in Fig. 4 for each type of specimen, at least two specimens were tested for each type and the averaged properties of the replicas are listed in Table 2.

Of all tensile curves shown in Fig. 4, the curve for DP980 BM has the highest ultimate tensile strength (UTS). The UTS of the DP980-DP980 joint was about 10% lower, as presented in Table 2. The average elongation of the welded specimens was only 3.0%, much lower than the 12.0% value of the BM. The elongation of the welded specimens showed a large standard deviation of 2.2% (see Table 2), contrary to the good repeatability (0.4%) exhibited by BM specimens. Fracture of the welded specimens initiated in the FZ near the BM where a sharp concavity often existed. Cracking then propagated into the softened zone (scHAZ) at about 45° angle in the thickness direction. The reduced plasticity and increased deviation were attributed to the concavity and other weld defects.

The tensile curve for HSLA BM, as shown in Fig. 4, exhibits excellent plasticity. The curve ended at 20% elongation simply because that was the range limit of the extensometer. Manual measurement gave an estimation of 24.7% elongation. The partial curve, however, included the peak stress (UTS = 520 MPa), which was reached at 13.5% strain. For HSLA-HSLA similar joint, the UTS and even the yield strength (YS) of the martensitic material in the FZ and ucHAZ were substantially higher than the UTS of HSLA BM. Because there was no softened zone, as shown earlier in Fig. 2, weldment did not present a weak location in tensile tests for HSLA. Moreover, as the applied stress was considerably lower than the YS of martensitic material, there was no plastic deformation in FZ and ucHAZ. The weldment thereby acted effectively as reinforcement in the specimen and prevented necking from occurring in its proximity. As a result, fracture always occurred in the HSLA BM away from the weldment. The tensile properties of the HSLA-HSLA similar joint were, therefore, very close to those of HSLA BM, with average UTS of 514 MPa and elongation of 22.3%.

For DP980-HSLA and DP980-HSLA-DP980 joints, due to the vast difference in tensile strength between DP980 and HSLA, the DP980 segment was undergoing elastic deformation



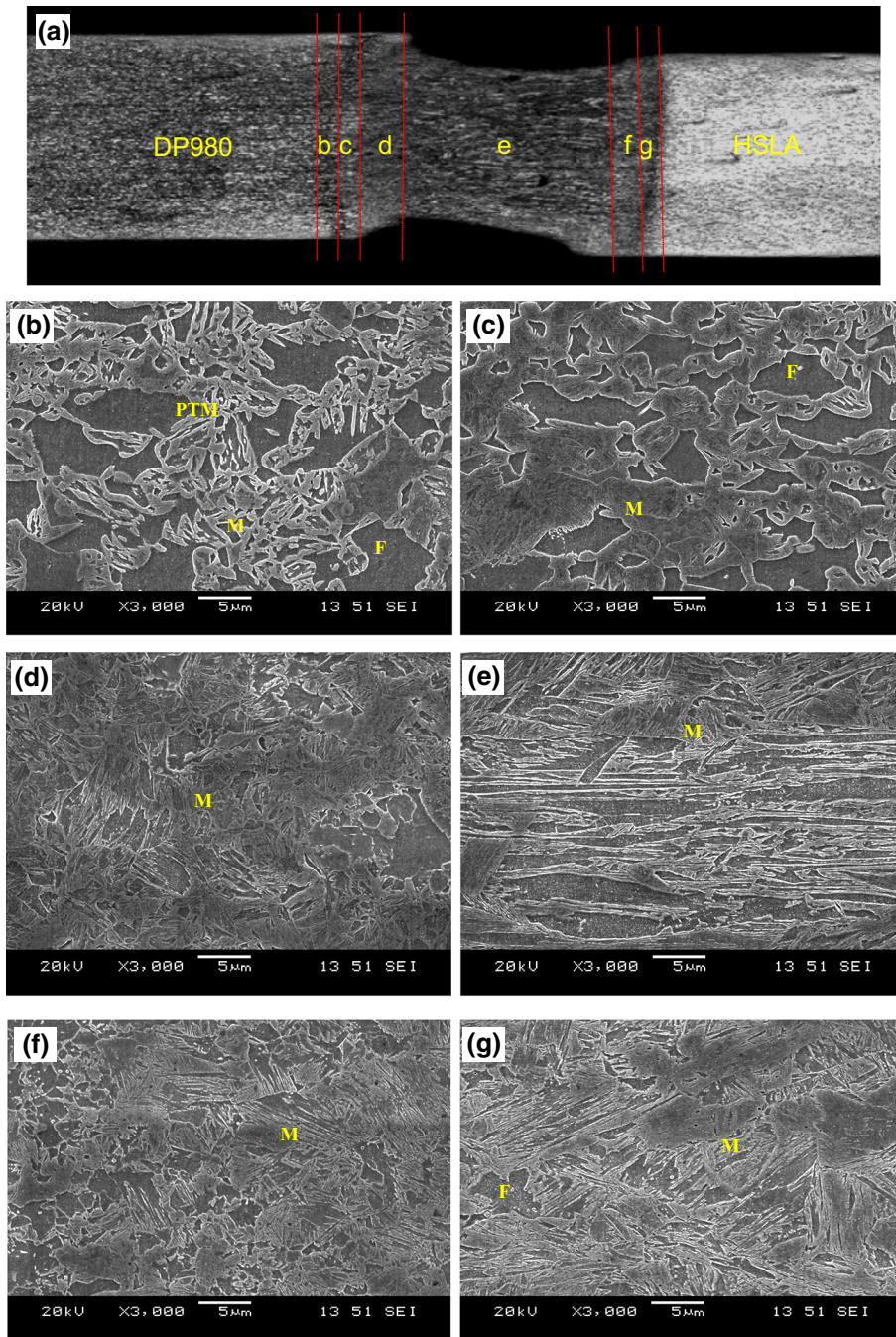


**Fig. 3** Microstructure of the DP980-HSLA dissimilar welding, (a) overall view, (b) DP980 sub-critical HAZ, (c) DP980 inter-critical HAZ, (d) DP980 upper-critical HAZ, (e) FZ, (f) HSLA upper-critical HAZ, (g) HSLA inter-critical HAZ (F: ferrite, M: martensite, PTM: partially tempered martensite)

when the HSLA segment reached its UTS. Tensile tests of those joint specimens were, thereby, essentially the tests of HSLA. Their tensile curves in Fig. 4 appeared different from that of HSLA BM simply because the extensometer measured both the deformed HSLA segment and the non-deformed DP980 segment. Assuming that the elongation of the HSLA segment remained at 24.7%, the apparent elongation for the DP980-HSLA and DP980-HSLA-DP980 joints can be calculated as 12.2 and 8.7%, respectively. These calculated values agreed reasonably well with experimental measurements of 13.8 and 9.7% in Table 2. As the nominal strain

rate was kept constant, the effective strain rate for the HSLA segment in the DP980-HSLA and DP980-HSLA-DP980 joints increased by 2.0 times and 2.9 times, respectively. These minor changes in the strain rate might have led to slight changes in tensile properties such as slightly higher UTS of 524 MPa for the DP980-HSLA-DP980 specimens.

### 3.3 Fatigue Properties

A common way to present the fatigue test results is by plotting the stress amplitude  $\sigma_a$  against the number of cycles to

failure  $N_f$  (Ref 18). With the stress ratio fixed at 0.1, the stress amplitude equals 0.45 times of the applied peak stress. The resulting plot thus produced is better known as the  $S-N$  plot. The  $S-N$  plots for DP980 BM, HSLA BM and four types of joints are shown in Fig. 5. As the graph is crowded with six groups of data points, adding trend lines helps to improve the clarity. The trend lines displayed in Fig. 5 represent the best fits to the Basquin equation (Ref 21),

$$\sigma_a = \sigma'_f (2N_f)^b \quad (\text{Eq 1})$$

where  $\sigma'_f$  is the fatigue strength coefficient and  $b$  is the fatigue strength exponent.

Note that the Basquin equation models the high-cycle fatigue where the nominal strain is elastic. Taking DP980 BM for instance (red squares in Fig. 5), the pair of data points at the highest  $\sigma_a$  of 450 MPa had a peak stress of 1000 MPa which was greater than the YS of DP980 BM (Table 2). Excluding this set of data points resulted in better fitting (higher  $R^2$ ). For a relatively low  $\sigma_a$  of 250 MPa, the endurance limit of the material was higher than that stress level, meaning that no crack could initiate and grow to a critical length such that crack propagation would continue under the cyclic load. Therefore, no failure occurred when the test was stopped after twelve million cycles. This set of data points was also excluded from the fitting. The resulting fitting ( $\sigma'_f = 1451$  MPa and  $b = -0.130$ , as listed in Table 2), displayed as a solid red line in Fig. 5, represents the three intermediate sets of data very well ( $R^2 = 0.94$ , also listed in Table 2). The fatigue strength coefficient  $\sigma'_f$  is comparable to UTS, while the fatigue strength exponent  $b$  has a reasonable value for high-strength steel.

Limited simultaneously by low YS and high fatigue strength, only three sets of data points (cyan squares in Fig. 5) were available for HSLA BM. The highest  $\sigma_a$  employed

was 250 MPa, which corresponded to 556 MPa peak stress, exceeding not only the YS but also the UTS of HSLA BM. At such a high stress level, the specimen would rapidly enter the last stage of fracture. Specimens managed to endure over 400 cycles primarily owing to the excellent plasticity (24.7% elongation as discussed earlier). At the stress level of 200 MPa, no failure occurred when the tests were terminated at over ten million cycles. Excluding these two sets of data points, only one data point (225 MPa) was within the applicable range of Basquin equation. Of course, no trend line can be drawn for a lone set of data points. Hence, no trend line is illustrated for HSLA BM in Fig. 5.

With high YS and low fatigue strength, DP980-DP980 joint was tested in a large span of  $\sigma_a$  ranging from 450 MPa down to 100 MPa (red diamonds in Fig. 5). For all specimens, cracking initiated in the FZ near the FZ/HAZ interface where residual thermal stress was the highest and the stress concentration was the greatest due to concavity. Weld defects might also directly aid the initial cracking. Compared to DP980 BM, the DP980-DP980 joint had lower  $N_f$ , attributable primarily to convenient crack initiation. As the stress amplitude decreased, the crack initiation became increasingly difficult for DP980 BM and eventually became unattainable at the stress level of 250 MPa. In contrast, even at very low stress levels crack initiation occurred readily in the welded joint, as will be revealed in detail by the fractography done in the following section. Thus, the difference in  $N_f$  between DP980 BM and the welded joint increased with decreasing stress amplitude. Another important factor contributing to the difference between the BM and the welded joint was that much of the fatigue damage of the joint occurred in the FZ where a brittle martensitic microstructure prevailed. It was difficult for brittle microstructure to arrest the crack tip, thus resulting in more rapid crack propagation (Ref

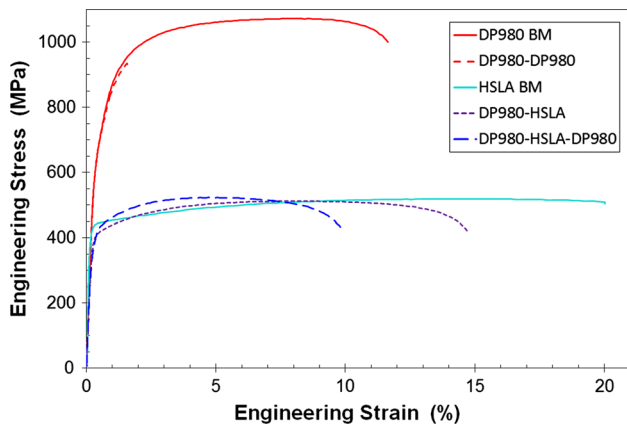


Fig. 4 Tensile curves of various types of welded joints between DP980 and HSLA

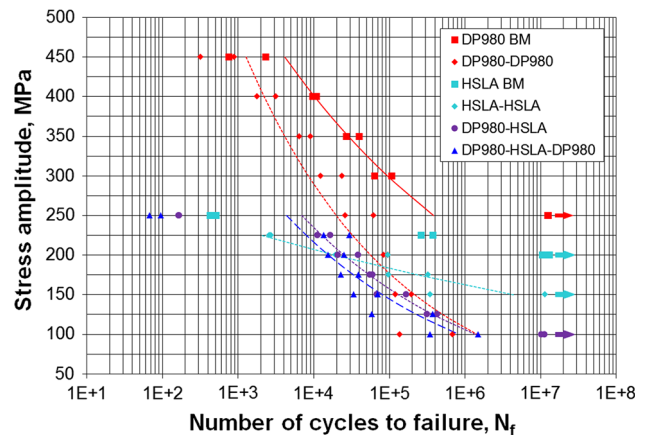


Fig. 5  $S-N$  curves of various types of welded joints between DP980 and HSLA

Table 2 Summary of tensile and fatigue properties

	YS, MPa	UTS, MPa	Elongation, %	Fatigue strength, MPa	Fatigue ratio	$\sigma'_f$ , MPa	$b$	$R^2$
BM DP980	707 ± 5	1083 ± 11	12.0 ± 0.4	250	0.231	1451	-0.130	0.94
BM HSLA	442 ± 3	520 ± 1	24.7	200	0.361	...	...	...
DP980-DP980	715 ± 20	972 ± 70	3.0 ± 2.2	< 100	< 0.094	2410	-0.214	0.84
HSLA-HSLA	407 ± 2	514 ± 4	22.3	< 150		350	-0.053	0.83
DP980-HSLA	427 ± 30	514 ± 17	13.8 ± 1.1	100	0.2	1309	-0.174	0.94
DP980-HSLA-DP980	420 ± 4	524 ± 1	9.7 ± 0.1	< 100	< 0.19	1222	-0.175	0.79



22). The advantage of hard microstructure in deterring crack initiation was, unfortunately, not realized because crack initiation in FZ was easy as discussed earlier. The low  $N_f$  value at low stress amplitudes led to a steep trend line (red dotted line in Fig. 5) with a very negative exponent  $b$  of  $-0.214$ . This very negative  $b$  value, in turn, resulted in a high intercept of  $\sigma'_f = 2410$  MPa, which was considerably higher than UTS (972 MPa).

Data points for HSLA-HSLA similar joint are shown as cyan diamonds in Fig. 5 together with a cyan dotted trend line ( $\sigma'_f = 350$  MPa and  $b = -0.053$ ). The slope of the trend line was very gentle ( $b = -0.053$ , typical for relatively soft materials) when compared to that of DP980-DP980 joint. These two trend lines thus crossed over. For  $\sigma_a \leq 175$  MPa or  $N_f \geq 10^5$  cycles, the HSLA-HSLA joint outlasted DP980-DP980 joint in the fatigue test. It is worth noting that for both types of similar joints, cracking initiated in FZ where martensitic microstructure was obtained for both HSLA and DP980. A major difference existed in the C content (0.08% for HSLA and 0.15% for DP980, as listed in Table 1); its effect was also reflected in Vickers hardness measurements as discussed earlier. The HSLA FZ might be slightly less brittle than the DP980 FZ, resulting in better performance at low stress amplitudes.

A DP980-HSLA dissimilar joint inherited the weakness from both types of steels. With the crossover of the trend lines of similar joints of these two steels, it was expected that the dissimilar joint would suffer a rapid fracture in the soft HSLA BM at  $\sigma_a \geq 250$  MPa while incurring failure in the FZ on the DP980 side at low  $\sigma_a$ . This was exactly what was observed in experiments. Experimental data plotted in Fig. 5 (purple circle dots with a purple dotted trend line) also confirmed the

hypothesis. Note that endurance limit of the dissimilar joint was 100 MPa, which was lower than the endurance limit of HSLA similar joint but higher than that of DP980 similar joint. A plausible explanation was that the chemistry of the FZ of the dissimilar joint was a result of the mixing of the two components.

The behavior of DP980-HSLA-DP980 multiple joint was related to that of the DP980-HSLA dissimilar joint. The fatigue life of DP980-HSLA-DP980 multiple joint (blue triangular dots with a blue dashed trend line in Fig. 5) was in general slightly shorter than the corresponding fatigue life of the DP980-HSLA counterpart, presumably attributable to the probabilistic feature of fatigue failure as the chance of having more severe weld defects increased with the number of weldments (one for the dissimilar joint and two for the multiple joint). For  $\sigma_a = 250$  MPa where the failure occurred solely inside HSLA BM and away from any weldments, the fatigue life of the multiple joint was slightly shorter than that of the dissimilar joint, which, in turn, was slightly shorter than that of HSLA BM. This trend might be explainable by the effective sample length (DP980 was rigid at that stress amplitude), which was 20 mm for the multiple joint, 28 mm for the dissimilar joint and 57 mm for the BM specimen. More localized straining exacerbated necking, thus accelerating the low cycle fatigue failure of the relatively soft HSLA steel (Ref 23).

### 3.4 Fractography

The fracture surface of a specimen records the entire fatigue process from crack initiation and initial stage I growth to the stage II steady crack propagation and eventually to the final rapid rupture. For a dissimilar joint or a multiple joint, the

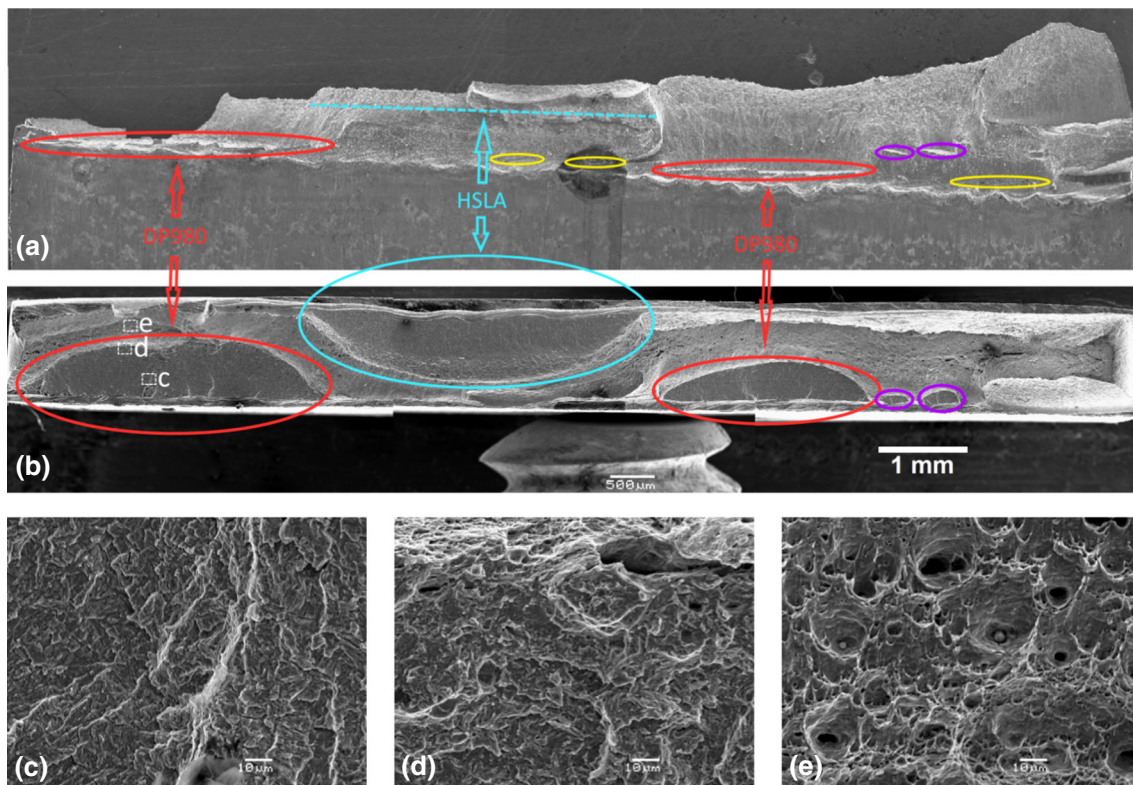


**Fig. 6** SEM images of fatigue fracture surface of a multiple joint tested at a stress amplitude of 225 MPa: (a) overall plane view, (b) overall cross-sectional view, (c) early stage II propagation region, (d) late stage II propagation region, and (e) rapid fracture region

behavior of different materials at different stages of the fatigue process makes the fractographic examination and analysis even more interesting.

The fracture surface of a DP980-HSLA-DP980 multiple joint specimen tested at  $\sigma_a = 225$  MPa ( $N_f = 29,660$  cycles) is shown in Fig. 6. Figure 6(a) shows the plane view of the fracture area with the top of the weldment facing the reader. The final rupture started from the left end of the weld close to DP980 and propagated to the right and slightly upward, first in the weldment and then entering the HSLA BM. The wavy FZ/DP980 border was easy to identify; the waviness was created due to the instability of the keyhole (laser was operated in continuous wavelength mode and was not pulsating). Much of the FZ/HSLA border was attached to the other half of the fractured specimen and is not displayed here. Only a short segment of the FZ/HSLA border can be seen at the right end of the weldment in Fig. 6(a). Figure 6(b) shows the cross-sectional view of the same fracture surface. It ought to be noted that the depth perception of SEM is often misleading. An experienced examiner relies on the work distance reading to judge the “altitude” of the fracture surface. In Fig. 6, the combination of the plane view and the cross-sectional view makes it easy to identify the locations of many important features. The most conspicuous features shown in Fig. 6 were three fatigue cracks. Each crack had a semi-oval shape with a length of a few millimeters and a width of about 1 mm. Two of these cracks (marked in red) were located in the FZ near the

DP980 border where weld concavity often caused stress concentration. These two cracks initiated from the top of the weld (front in Fig. 6a or the lower edge in Fig. 6b) and propagated toward the bottom of the weld as they widened. Conversely, the other crack initiated from the back (thus marked as a cyan dashed line in Fig. 6a) near the FZ/HSLA border. All three cracks propagated in planes perpendicular to the loading direction, bearing characteristics of stage II cracking. No crack initiation areas were found, probably because cracks could initiate readily from weld defects such as concavity. Easy crack initiation was in agreement with the low fatigue endurance limit (fatigue strength) of these welded specimens as shown previously in Fig. 5. Close examination of the two cracks marked in red revealed small ridges (Fig. 6b) close to the weld surface. These ridges were formed in early stage II propagation when small cracks initiated at slightly different levels merged to form a large crack. This is comprehensible by cross-examining the fine features in Fig. 6(a) and (b). More details of the boxed area marked as “c” in Fig. 6(b) are revealed in the micrograph shown in Fig. 6(c). No apparent fatigue striations are shown in the brittle martensitic material due to the absence of plastic blunting of the crack tip. Figure 6(d) shows the transition area from steady crack propagation to final rapid fracture. Figure 6(e) displays more ductile deformation with characteristic dimple features in the final rupture area. The final rupture proceeded from left to right (Fig. 6b) along the wavy corridor between three semi-oval

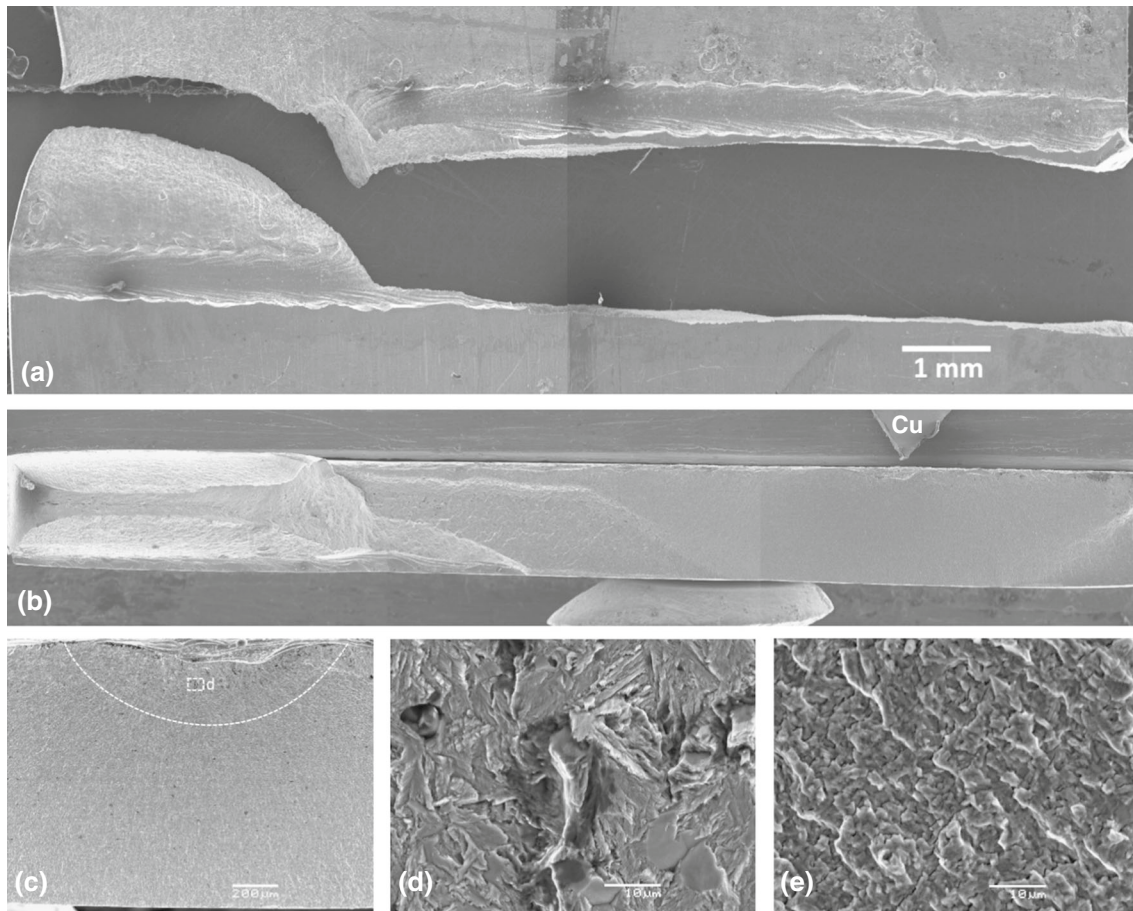


**Fig. 7** SEM images of fatigue fracture surface of a multiple joint tested at a stress amplitude of 100 MPa: (a) overall plane view, (b) overall cross-sectional view, (c) crack initiation area, (d) stage I crack growth, and (e) stage II crack growth



fatigue cracks, and eventually advanced into the HSLA BM. The final rupture in HSLA BM bores great similarity to the fracture that occurred in the tensile testing of HSLA BM and welded specimens.

In addition to the three large fatigue cracks, two smaller cracks are marked with purple ovals in Fig. 6(a) and (b). Upon close examination, additional cracks that were not exposed on the fracture surface (Fig. 6b) are visible in the plane view (circled with yellow ovals in Fig. 6a). Cracks are also visible on the other weldment in this multiple joint specimen. Long before the specimen succumbed to final fracture, severe damage had incurred as multiple cracks substantially propagated at various locations.

It is conceivable that a specimen tested at low  $\sigma_a$  can behave much differently from one tested at high  $\sigma_a$ . A DP980-HSLA-DP980 multiple joint specimen tested at a low  $\sigma_a = 100$  MPa ( $N_f = 1.5 \times 10^6$  cycles) was carefully examined. One large single fatigue crack was found at the FZ/DP980 interface as shown in Fig. 7(a) and (b), in sharp contrast to the many fatigue cracks found on the specimen tested at a high  $\sigma_a = 225$  MPa. Also, it was different from the specimen tested at high  $\sigma_a$  where no apparent crack initiation area was detectable; one crack initiation area was visible to the unaided eye on the low  $\sigma_a$  specimen. A Cu ribbon tape was placed next to this area for easy positioning under SEM, as shown in Fig. 7(b). A large weld defect was found and is shown in a higher magnification in Fig. 7(c). Note that the lower edge of Fig. 6(c) (also Fig. 7b) is the top side of the weldment, which is facing the reader in Fig. 7(a). Thus, the weld defect on the upper edge in Fig. 7(c) was on the bottom side of the weldment and might be produced by insufficient penetration of the keyhole at that particular location. Surrounding the weld defect is an area that appeared to the naked eye to have a lighter contrast; this reflection contrast was hardly cognizable under SEM probably because the secondary electrons (or backscatter electrons) bent their trajectories toward the electron detector. The approximate border of this lighter contrast area is marked with a dashed line in Fig. 7(c). The fracture surface in this area appeared rougher under SEM, likely resulting from the initial stage I propagation. Detail of a selected area in Fig. 7(c) is shown in Fig. 7(d). Although martensitic microstructure was ubiquitous in FZ, one bundle of lath martensite was particularly evident near the top center of the micrograph. Smooth planes intersecting at angles of about  $120^\circ$  near the bottom center of the micrograph greatly resembled the boundaries of prior austenite grains. The entire area was notably rougher than a normal area (stage II propagation, as shown in Fig. 7e) a couple millimeters away. The presence of the crack initiation and stage I growth area highlight the increased difficulty of crack initiation under low  $\sigma_a$ . The difficulty of crack initiation limited the number of cracks, explaining why single fatigue crack was found on specimens tested at low  $\sigma_a$ , whereas multiple cracks formed on specimens tested at high  $\sigma_a$ . Although the crack initiated in FZ, it propagated toward DP980 in stage I growth. Almost the entire stage II growth took place in uHAZ of DP980, which was even harder and likely more brittle than the FZ (Fig. 2). It is evidently shown in Fig. 6(a) that a thin slice of less than 0.2 mm of DP980 was attached to the FZ in the upper half of the fractured specimen. Referring to the thickness of uHAZ marked in Fig. 2, it can be concluded that the stage II crack propagation took place inside the uHAZ. It is worth noting that, for the test with  $\sigma_a = 100$  MPa, when the crack propagated to about one half of the cross section (Fig. 7b), the effective  $\sigma_a$

would double to about 200 MPa, which would be high enough to activate many fatigue cracks in the weldments. However, the stress intensity factor of the major crack would be much greater than that of nascent cracks due to the prominent length of the major crack. As a matter of fact, the stress intensity factor of the major crack had approached  $K_{IC}$  (critical stress intensity factor for type I cracks); the fatigue process thus started to enter the rapid fracture stage. As shown in Fig. 7(b), the fracture surface started to exhibit features of rapid ductile rupture. Cracking then abruptly broke through the weld and propagated deep into HSLA BM, as shown in Fig. 7(a).

The fracture surface was almost identical for the duplicate specimen also tested at  $\sigma_a = 100$  MPa ( $N_f = 3.5 \times 10^5$  cycles). One dominant crack initiated from the top of the weldment at the FZ/DP980 interface. Cracking then propagated in uHAZ of DP980 during its stage II growth. It is worth noting that whereas multiple cracks were activated from both DP980 side and HSLA side in dissimilar and multiple joint specimens at high  $\sigma_a$ , one dominant crack typically formed from the more brittle DP980 side at low  $\sigma_a$ . Moreover, the weakest path for crack propagation at low  $\sigma_a$  appeared to be the material with highest hardness (likely most brittle), which was the uHAZ of DP980. At high  $\sigma_a$ , cracks opted to propagate into the soft material, which was the HSLA BM. These observations agreed very well with the fatigue life of DP980 and HSLA at different  $\sigma_a$ , highlighted by the crossover of their trend lines shown in Fig. 5.

## 4. Conclusions

The microstructure, hardness profile, tensile properties and fatigue performance of multiple and single dissimilar fiber laser-welded joints of DP980-HSLA were presented. The major conclusions that can be drawn from this work are as follows:

1. Dissimilar DP980-HSLA joints welded by fiber laser had a relatively narrow FZ of about 0.6 mm, the microstructure of which was fully martensitic. On the HSLA side, the HAZ was quite narrow (about 0.3 mm) with the microhardness rapidly decreasing from the peak value to the normal hardness of BM in the absence of a softened zone. On the DP980 side, the uHAZ was relatively wide (about 0.2 mm) with the microhardness plateauing at the peak value owing to a fully martensitic microstructure. The softened zone, which encompassed the scHAZ and part of the icHAZ, was very wide (about 0.6 mm). The degree of softening was also substantial (240 HV compared to over 300 HV for DP980 BM).
2. Because the UTS of HSLA was considerably lower than the YS of DP980, the DP980 segment was in the elastic deformation regime throughout the tensile test. Even the softened zone of DP980 did not appear to incur any plastic deformation. Thus, all plastic deformation took place in the HSLA segment, and the failure always occurred in HSLA BM away from the weldment.
3. In the fatigue test, DP980 BM specimens survived ten million cycles at stress amplitude of 250 MPa, while HSLA BM had an endurance limit of 200 MPa. The endurance limit of HSLA-HSLA similar weld was just below 150 MPa. The endurance limit of DP980-DP980 similar weld was, however, not obtainable even at low



stress amplitude of 100 MPa. The low endurance limit of welded specimens was attributed to easy crack initiation in FZ at the FZ/HAZ interface where concavity and other weld defects existed and significant stress concentration presented. DP980-DP980 joints outperformed HSLA-HSLA joints at high stress amplitude but fared worse at low stress amplitude.

4. For DP980-HSLA dissimilar joint and DP980-HSLA-DP980 multiple joint, the performance at high stress amplitude (250 MPa) was limited by the strength of HSLA. At stress amplitudes lower than the fatigue strength of HSLA welded sample (below 125 MPa), a single fatigue crack initiated in FZ at the FZ/DP980 border and then propagated in ucHAZ of DP980 where the hardness was the highest (likely most brittle). At intermediate stress amplitudes, multiple cracks typically initiated in FZ on both FZ/DP980 and FZ/HSLA borders. Steady crack propagation took place in FZ along both borders. Final rapid fracture always occurred in HSLA BM due to its low UTS.

## Acknowledgments

The authors would like to thank the National Natural Science Foundation of China (No. 51304045), the China Scholarship Council (CSC), Natural Sciences and Engineering Research Council of Canada (NSERC) and AUTO21 Network of Centers of Excellence for providing financial support. The financial support from International Zinc Association (IZA) and Arcelor-Mittal Dofasco is highly acknowledged. One of the authors (D.L.Chen) is grateful for the financial support by the Premier's Research Excellence Award (PREA), NSERC-Discovery Accelerator Supplement (DAS) Award, Canada Foundation for Innovation (CFI), and Ryerson Research Chair (RRC) program. The authors would like to thank Dr. J. Chen and Dr. Y.L. He (CANMET-Materials Technology Laboratory, Natural Resources Canada, Hamilton, Canada), Mr. E. Biro (ArcelorMittal Global Research, Hamilton, Canada), and Dr. J. Villafuerte (CenterLine (Windsor) Ltd., Windsor, Canada) for their support and helpful discussion. The assistance of Q. Li, A. Machin, J. Amankrah, and R. Churaman in performing the experiments is gratefully acknowledged.

## References

1. G.K. Ahiale and Y. Oh, Microstructure and Fatigue Performance of Butt-Welded Joints in Advanced High-Strength Steels, *Mater. Sci. Eng. A*, 2014, **597**, p 342–348
2. Q. Jia, W. Guo, P. Peng, M. Li, Y. Zhu, and G. Zou, Microstructure and Strain Rate-Dependent Tensile Behavior of Fiber Laser-Welded DP980 Steel Joint, *J. Mater. Eng. Perform.*, 2016, **25**, p 668–676
3. D. Anand, D.L. Chen, S.D. Bhole, P. Andreychuk, and G. Boudreau, Fatigue Behavior of Tailor (Laser)-Welded Blanks for Automotive Applications, *Mater. Sci. Eng. A*, 2006, **420**, p 199–207
4. J.H. Lee, S.H. Park, H.S. Kwon, G.S. Kim, and C.S. Lee, Laser, Tungsten Inert Gas, and Metal Active Gas Welding of DP780 Steel: Comparison of Hardness, Tensile Properties and Fatigue Resistance, *Mater. Des.*, 2014, **64**, p 559–565
5. Y.Y. Zhou, Y.S. Zhang, and W. Hu, Effect of Welding Speed on Microstructure, Hardness and Tensile Properties in Laser Welding of Advanced High Strength Steel, *Sci. Technol. Weld. Join.*, 2013, **18**(7), p 581–590
6. A.P. Pierman, O. Bouaziz, T. Pardoen, P.J. Jacques, and L. Brassart, The Influence of Microstructure and Composition on the Plastic Behaviour of Dual-Phase Steels, *Acta Mater.*, 2014, **73**, p 298–311
7. D. Westerbaan, D. Parkes, S.S. Nayak, D.L. Chen, E. Biro, F. Goodwin, and Y. Zhou, Effect of Concavity on Tensile and Fatigue Properties in Fiber Laser Welding on Automotive Steels, *Sci. Technol. Weld. Join.*, 2013, **19**, p 60–68
8. D. Parkes, W. Xu, D. Westerbaan, S.S. Nayak, Y. Zhou, F. Goodwin, S. Bhole, and D.L. Chen, Microstructure and Fatigue Properties of Fiber Laser Welded Dissimilar Joints Between High Strength Low Alloy and Dual-Phase Steels, *Mater. Des.*, 2013, **51**, p 665–675
9. W. Xu, D. Westerbaan, S.S. Nayak, D.L. Chen, F. Goodwin, and Y. Zhou, Tensile and Fatigue Properties of Fiber Laser Welded High Strength Low Alloy and DP980 Dual-Phase Steel Joints, *Mater. Des.*, 2013, **43**, p 373–383
10. D. Westerbaan, S.S. Nayak, D. Parkes, W. Xu, D.L. Chen, S.D. Bhole, F. Goodwin, E. Biro, and N. Zhou, Microstructure and Mechanical Properties of Fiber Laser Welded DP980 and HSLA Steels, *Proceedings of SMCX XI*, Detroit, MI, USA, vol. 3 (2012), pp. 1–13
11. J. Canning, Fiber Lasers and Related Technologies, *Opt. Lasers Eng.*, 2005, **44**, p 645–676
12. E. Assuncao, L. Quintino, and R. Miranda, Comparative Study of Laser Welding in Tailor Blanks for the Automotive Industry, *Int. J. Adv. Manuf. Technol.*, 2012, **49**, p 123–131
13. B. Rooks, Tailor-Welded Blanks Bring Multiple Benefits to Car Design, *Assem. Autom.*, 2001, **21**, p 323–328
14. D. Parkes, Q.L. Cui, D. Westerbaan, S.Nayak, Y. Zhou, F. Goodwin, D. Liu, S. Bhole, and D.L. Chen, Effect of Fiber Laser Welding on the Fatigue Properties of Dissimilar Welded Joints Between DP980 and HSLA Steels. SAE International. 01-0990 (2014)
15. N. Farabi, D.L. Chen, and Y. Zhou, Tensile Properties and Work Hardening Behavior of Laser-Welded Dual-Phase Steel Joints, *J. Mater. Eng. Perform.*, 2012, **21**, p 222–230
16. W. Xu, D. Westerbaan, S.S. Nayak, D.L. Chen, F. Goodwin, E. Biro, and Y. Zhou, Microstructure and Fatigue Performance of Single and Multiple Linear Fiber Laser Welded DP980 Dual-Phase Steel, *Mater. Sci. Eng.*, 2012, **553**, p 51–58
17. M. Xia, E. Biro, Z. Tian, and Y. Zhou, Effects of Heat Input and Martensite on HAZ Softening in Laser Welding of Dual Phase Steels, *ISIJ Int.*, 2008, **48**, p 809–814
18. Q.L. Cui, D. Parkes, D. Westerbaan, S.S. Nayak, Y. Zhou, D. Liud, F. Goodwin, S. Bhole, and D.L. Chen, Effect of Coating on Fiber Laser Welded Joints of DP980 Steels, *Mater. Des.*, 2016, **90**, p 516–523
19. B. Yin, L.P. Li, Y. Zhou, L. Gong, M.B. Yang, and B.H. Xie, Largely Improved Impact Toughness of PA6/EPDM-g-MA/HDPE Ternary Blends: The Role of Core-Shell Particles Formed in Melt Processing on Preventing Micro-Crack Propagation, *Polymer*, 2013, **7**, p 1938–1947
20. Y. Liu, Y.M. Wang, and L. Liu, Fatigue Crack Propagation Behavior and Fracture Toughness in a Ni-Free ZrCuFeAlAg Bulk Metallic Glass, *Acta Mater.*, 2015, **92**, p 209–219
21. G.E. Dieter, *Mechanical Metallurgy*, 3rd ed., McGraw-Hill, New York, 1986
22. M. Brede, K.J. Hsia, and A.S. Argon, Brittle Crack Propagation in Silicon Single Crystals, *J. Appl. Phys.*, 1991, **70**, p 758–771
23. K.H. Nip, L. Gardner, C.M. Davies, and A.Y. Elghazouli, Extremely Low Cycle Fatigue Tests on Structural Carbon Steel and Stainless Steel, *J. Constr. Steel Res.*, 2010, **66**, p 96–110